Raman scattering applied to human breath analysis

Charuka Muktha Arachchige and Andreas Muller

Department of Physics, University of South Florida

August 10, 2024

Abstract

The chemical composition of exhaled human breath can be strongly correlated to medical conditions such as lung cancer or gastrointestinal diseases. To establish these correlations and, most importantly, to use them in diagnostics, chemical gas detection needs to be performed at trace concentrations, typically at parts-per-million (ppm) levels or below, for many compounds simultaneously. Traditional methods such as gas chromatography, a workhorse in scientific laboratories, is ill-suited for the fast, inexpensive point-of-care diagnostics that would be needed to build statistically-meaningful ensembles over large populations. With the increasing availability and decreasing cost of high power diode lasers and of uncooled CMOS cameras, spontaneous Raman spectroscopy (SRS), a vibrational molecular fingerprinting tool, is emerging as an economic alternative. Although gas SRS scattering cross sections are only on the order of 10^{-31} cm^2/sr, considerable progress in the development of enhancement techniques has been made over the past decade. The purpose of this work is to review SRS enhancement approaches in the context of established human breath tests, and to provide a comparison with alternatives. Already, numerous trace gases such as H_2, CH_4, $^{13}CO_2$, and volatile organic compounds like acetone can be rapidly quantified in breath at concentrations below 1 ppm with SRS. With improvements in resolution and design of enhancement systems, SRS-based sensors could be scalably deployed in, e.g., pharmacies, and non-invasively screen for dozens of analytes at the parts-per-billion level.

1 Introduction

An organism's exhaled breath provides a most direct and non-invasive access to its volatilome, i.e., the ensemble of organic and inorganic volatile compounds that originate in its biochemical activity. The chemical composition analysis of exhaled breath thus provides a link to internal metabolic pathways with potential for disease diagnostics. Human breath analysis can be traced back to the time of Hippocrates, who advised his students to identify diseases by the smell of exhalates. Fruity smells would indicate symptoms of diabetes whereas a fishy smell may point to problems in the liver [1]. In the 1970s, Pauling made a remarkable breakthrough, discovering more than 200 volatile organic compounds (VOCs) in exhaled breath, leading to modern breath analysis [2]. With improvements in technology and analytical methods, numerous clinical studies have examined the underlying connections between breath VOCs and a patient's health [3]. Exhalation being controlled by the respiratory system, the primary focus was initially on the identification of lung cancers as well as asthma, tuberculosis, etc. [4].

Human breath consists of a mixture of endogenous (internally generated) and exogenous (externally introduced) trace chemicals in a background of primarily nitrogen (N_2), oxygen (O_2), carbon dioxide (CO_2), water vapor (H_2O), and argon (Ar). Inhaled air enters the alveoli of the lungs, where waste products from metabolic activity move into it [5]. These waste products are eventually released with exhaled air, as are other compounds that originate in biological processes other than those taking place in the lungs, such as digestion. Exogenous trace compounds in breath typically have their origin in the surrounding ambient air as, e.g., air pollutants. Most trace compounds are found at concentrations of order 10 parts-per-billion or less, with some notable exceptions, listed in Table 1, which are typically founds at concentrations of order parts-per-million. Challenges facing breath analysis as a diagnostic technique include the difficulty of quantifying a large set of analytes at widely differing concentrations, but also their considerable variations affected by a number of factors including age, gender, diet, habits, and physiological conditions. Today, medical practice administers some standardized tests such as the hydrogen breath tests or the urea test which involves the ingestion of isotopically-labeled food. With more widely deployed chemical analysis and improved statistical methodologies— possibly aided by machine learning to identify correlations in large data sets— new breath diagnostics are poised to emerge.

Table 1: Predominant trace gases found in exhaled breath and associated diagnostics

Gas	**Inhaled**	**Normal exhaled**	**Abnormal exhaled**	**Diagnosis**	**Reference**
Carbon dioxide (CO_2)	0.04%	3%-4%	-	Respiration monitoring	[6–8]
Carbon monoxide (CO)	0.25 ppm	0.5-2.1 ppm	16.7-29.3 ppm	Chronic obstructive Pulmonary disease(COPD)	[9]
			5.6 ppm	Asthmatic patients	[10]
			4.4 ppm	Hemolysis	[11]
Hydrogen (H_2)	0.5ppm	<5 ppm	> 20 ppm increase	Gastrointestinal disease	[12]
Methane (CH_4)	1.7 ppm	<1 ppm	>16 ppm increase	Diverticulitis, constipation irritable bowel syndrome	[13]
Acetone (C_3H_6O)	-	0.3 -1 ppm	2200 - 21000 ppb	Diabetes mellitus Ketosis	[14, 15]
Ammonia (NH_3)	-	50-1500 ppb	1500 - 15000 ppb	Renal failure Chronic kidney disease	[16–19]

Here we review the literature on spontaneous Raman spectroscopy applied to the trace identification and quantification of analytes relevant to breath analysis. A technique best known for non-invasive characterization of liquids and solids, for example in the pharmaceutical industry, SRS has been employed much less to the widespread chemical analysis of gases. SRS relies on inelastic scattering by which a molecule's vibrational frequencies—its molecular fingerprint—are imparted onto incident pump light. The resulting photon flux of so-called "Stokes photons", that is collected and spectrally analyzed, is relatively low. In fact, Raman scattering cross sections are orders of magnitude lower than those involved in, e.g., fluorescence processes. For this reason, SRS gas spectroscopy, although extensively developed in the 1970s and 1980s, has remained a specialized laboratory tool until recently, when high power lasers, sensitive array detectors, and other high-performance optical components have become widely available commercially. The review is organized as follows. First, a brief survey of the most relevant breath markers is provided, followed by the description of established breath tests. Traditional trace gas analyzers are then described including those that are currently most commonly used for breath analysis as well as alternatives being actively researched. Raman spectroscopy techniques are then introduced together with the enhancement methods that have been investigated the most. Case uses that are pertinent to breath analysis are covered in detail, and perspectives are presented in view of potential future improvements.

2 Background

Human breath contains a great number of organic and inorganic compounds which can be categorized into five main groups. Large quantities of ***saturated hydrocarbons*** (e.g., ethane, pentane)

can be generated as a result of oxidation of fatty acids and proteins. ***Unsaturated hydrocarbons*** such as isoprene are known to be fundamental components of the mevalonic pathway. Among ***oxygen-containing compounds***, acetone is the most abundant in human breath. ***Sulphur-containing compounds*** are produced when methionine is not properly metabolized via the transamination pathway. The most important ***nitrogen-containing volatile*** biomarker is ammonia, a breakdown product of proteins [3, 5, 20].

Biological processes in the human body are nonlinear and dynamic, with considerable dependence on genetic conditions, environmental factors, and nutrition. Understanding the variations in breath compounds from their healthy baseline levels is crucial for disease diagnosis and monitoring.

2.1 Established breath tests

Breath tests are designed to diagnose specific physiological health conditions. They are based on the determination of the concentration of one or several analytes in exhaled breath relative to a baseline concentration. In general, the tests are more definitive the more elevated the detected concentrations.

2.1.1 Isotope urea breath test

The purpose of the urea breath test (UBT) is to detect an overabundance of the Helicobacter pylori (H. pylori) bacterium in the stomach or duodenum. H. pylori infection plays a substantial role in the onset of chronic gastritis and gastroduodenal ulcers and is strongly linked to the risk of developing gastric cancer. In the UBT, patients ingest ^{13}C-enriched urea which H. pylori metabolizes into ammonia and carbon dioxide. Thus, exhaled breath excessively rich in $^{13}CO_2$ shortly after administering ^{13}C-rich urea is a strong indication of an H. pylori infection. The successful implementation of the UBT hinges upon the precise determination of the isotopologue concentration ratio χ_{13_C}/χ_{12_C}, where χ_{13_C} and χ_{12_C} are volume fractions of the respective isotope. The natural χ_{13_C}/χ_{12_C} ratio of around 1% serves as a baseline [21].

During the UBT, a first breath sample is collected in a sealed bag following an overnight fast, serving as the baseline sample. Then, patients consume a beverage such as ordinary orange juice to which ^{13}C-urea (75 mg) has been added. After 30 minutes have passed an exhaled air sample is collected as the post-dose sample. If the concentration of ^{13}C in the post-dose breath sample exceeds the baseline sample by 30-40 permille an H. pylori infection is diagnosed, with higher levels suggesting a more extensive infection [22].

2.1.2 Hydrogen breath test

Due to its non-invasive nature, the hydrogen breath test (HBT) is the most widely administered clinical breath test. During the process of carbohydrate fermentation, hydrogen gas is released by bacteria in the bowel. This process only stands if unabsorbed carbohydrates stay as undigested material and are

allowed to move through the digestive tract from the small intestine into the large intestine. Produced hydrogen gas becomes a source of methane in the bowel also [23, 24]. These two gases are analyzed in the exhaled breath [23].

The HBT test is meant to diagnose physiological conditions such as bacterial overgrowth in the small bowel, a condition commonly referred to as small intestinal bacterial overgrowth (SIBO). Targeted assessments can be made by way of ingestion of specific sugars such as lactose, sucrose, fructose, and sorbitol. The HBT involves detecting hydrogen gas in exhaled breath at the ppm level, and tests are generally regarded as positive when detected hydrogen levels reach 10-20 ppm.

2.2 Trace gas analysis techniques

Although the UBT and HBT constitute established clinical tests, they both ultimately rely on trace gas detection capabilities that are not trivial. In the case of the UBT, isotopologue selectivity is required, i.e., the measurement technique must be able to detect the presence of a single extra neutron in CO_2. Furthermore, even if this capability is met, the relative concentration of the two isotopologues must be quantifiable with unusually high precision, i.e., to better than 1 percent. Not many chemical diagnostic tools are available to carry out such a task in an economical manner and we provide a brief survey in the following sections.

2.2.1 Ion-based detection methods

General-purpose trace breath analysis has traditionally been achieved almost exclusively using mass spectrometry (MS) assisted by supplemental methods. MS, which is based on the dispersion of ions by electromagnetic fields according to their mass-to-charge ratio, thereby functions as a highly discriminatory filter with very high detection sensitivity (ppb and below) [25, 26].

In gas chromatography-mass spectrometry (GC-MS), a chromatographic column, typically a long capillary tube, is employed in such a way as to separate analytes by their column retention time. A chromatogram is produced as a result of sequential detection at the end of the column by MS [27, 28].

The proton-transfer reaction-mass spectrometry (PTR-MS) concept was developed in the 1990s to isolate atmospheric VOCs by proton-transfer reactions with ions of H_3O^+. It employs a drift tube in which VOCs with a greater proton affinity than H_2O can undergo ionization through proton transfer to H_3O^+ ions [29]. A large number of target compounds can be detected and monitored concurrently for a specified mass range [1, 5, 29, 30].

In selected ion flow tube-mass spectrometry (SIFT-MS), reagent ions (H_3O^+, NO^+, O_2^+) generated in an ion source are used to ionize compounds through soft chemical ionization [31]. The reagent ions are filtered based on their mass-to-charge ratio using a quadrupole and a carrier gas (helium or nitrogen) moves rapidly through the flow tube. These reagent ions undergo a reaction with the gaseous sample (in this case, breath), and characteristic product ions are then analyzed by MS. Polar substances like

acetone, ammonia, and unsaturated hydrocarbons like isoprenes can be detected in a very accurate manner by SIFT-MS at ppt/pptv and ppb/ppbv ranges [1, 5].

Ion mobility spectrometry (IMS) involves the travel of ionized analytes under the influence of an electric field within a buffer gas [32]. IMS is an accurate technique able to differentiate volatile compounds even at low concentrations (ppm - ppb), simultaneously, according to their specific mobility [33]. Even though standalone IMS is powerful, it can be coupled with GC and MS. IMS is able to quantify distinct combinations of VOCs and is thus well-suited for breath analysis [5].

2.2.2 Optical absorption

Absorption spectroscopy relies on the property of molecules to absorb light at specific wavelengths [34, 35]. A molecule's characteristic fingerprint encompasses ultraviolet absorption features (electronic transitions) [36], as well as visible to infrared absorption features associated with molecular rotation and vibration degrees of freedom [37–39]. Molecular analytes relevant to breath analysis exhibit strong rotational-vibrational absorption characteristics in the mid-infrared. A host of optical absorption techniques have been researched and perfected over the years, such as, cavity ring-down absorption spectroscopy (CRDS) [40–43], off-axis integrated cavity output spectroscopy (ICOS), and quantum cascade tunable infrared laser differential absorption spectroscopy (QC-TILDAS) [44]. The maturity of these techniques is such that they are employed in commercial instruments for a variety of applications. Non-dispersive infrared (NDIR) sensors for single analytes are particularly widespread. Recently, CRDS has demonstrated unprecedented isotopologue sensitivity with the implementation of radio carbon measurements, [45] traditionally performed primarily by isotope ratio mass spectrometry (IRMS) [46]. Infrared spectrometry emerges as the most frequently employed technique for the UBT. This choice is predominantly driven by the instrument's notable attributes: its portability, affordability, and capacity for real-time analysis with high precision [47].

However, in the context of general-purpose breath analysis, optical absorption is not always adequate. In particular, homonuclear diatomic molecules such as hydrogen cannot be detected, which makes the HBT inaccessible. Additionally, a tunable laser source is often needed in practice, which constrains the available spectral range of detection, and thus the number of analytes that can be detected simultaneously.

2.2.3 Electrochemical sensors

Electrochemical sensors (EC) are compact and packaged sensor systems, utilizing catalysts or enzymes immobilized on electrodes to selectively identify and quantify analytes [48–50]. EC sensors are part of a wider family of sensors that also includes, e.g., electromechanical devices. The latter makes use of micromechanical (MEMS) resonators or surface acoustic waves to indirectly probe small frequency changes which have their origin in minute mass changes due to adsorbed analytes. The underlying disadvantage of these sensors is the indirect nature by which concentration determination occurs, requiring

recurrent calibration and suffering from poor specificity.

3 Spontaneous Raman scattering

Spontaneous Raman scattering is an inelastic light-matter interaction in which energy is exchanged between incident light and an internal excitation within a solid, liquid, or gas. For a gas, the relevant excitations are molecular rotations and molecular vibrations, which are quantized and unique to a particular analyte, thus providing a spectral fingerprint that can be detected in the generated scattered light. This is the basis for spontaneous Raman spectroscopy (SRS). Energy can be given to the molecule at the expense of the light (Stokes scattering), or taken from the molecule and given to the light (anti-Stokes scattering). We focus here exclusively on Stokes SRS, which leads to scattered light that has components at longer wavelengths than the incident light. The most basic SRS setup consists of a near-monochromatic light source focused into a gas sample, a set of optical elements to collect and filter the scattered light, and a spectrometer for spectral analysis. SRS spectra are typically reported as the rate of scattered photons (or the corresponding power), as a function of Raman shift $\Delta\bar{\nu}_R$. The latter, denoted in cm^{-1}, is defined as the difference between the pump laser frequency and the Stokes frequency, i.e., the frequency of the scattered light.

The rate of spontaneous Raman scattering depends linearly on the molecular number density, N/V, and thus the concentration, according to

$$\gamma_R = \varepsilon P_{pump} \frac{N}{V} l_{eff} \frac{d\sigma_R}{d\Omega}, \tag{1}$$

where ε is a proportionality constant that accounts for detection efficiency, P_{pump} the incident laser power, N the number of molecules, V the volume, l_{eff} the effective interaction length, and $d\sigma_R/d\Omega$ the Raman differential scattering cross section of the analyte [51]. For vibrational SRS near room temperature and for $\Delta\bar{\nu}_R \gg 100\ \mathrm{cm}^{-1}$, molecules can be assumed thermalized in their vibrational ground state, and any temperature dependence of γ_R may be ignored [52].

Taking exception of vacuum field effects, the scattering cross section $d\sigma_R/d\Omega$ is fixed for a particular molecular vibration in a given analyte [53]. For gases it is on the order of only $10^{-31}\ \mathrm{cm}^2/\mathrm{sr}$ but scales with the fourth power of the Stokes frequency [54]. Thus, bluer pump light is generally preferable over redder pump light. Cross sections vary between analytes and modes of vibration but are mostly on the same order of magnitude for the dominant bands. For example, for the gases listed in Table 1, the smallest cross section (CO) differs from the largest (CH_4) by a factor of only 7. At the molecular level, the cross section is determined by the rate of change of the polarizability with the relevant normal coordinate.

Gases under atmospheric conditions are nearly three orders of magnitude less dense than solids or liquids. For moderate pump powers of, say, hundreds of milliwatt, and for a free-space configuration,

one finds scattering rates γ_R on the scale of only millions of photons per second, requiring high-efficiency low-noise detection and stringent suppression of background light. Consequently, practical applications of SRS have been, until recently, largely limited to probing concentrated gases, for example, in industrial processes. However, considerable progress has been made over the past decade to make SRS useful for trace gas sensing also. Broad research efforts have been devoted to devising enhancement methods with the purpose of increasing γ_R in Eq. (1), by way of P_{pump}, N/V, or l_{eff}.

3.1 Enhancement by pressurization

The most straightforward way to raise the rate in Eq. (1) is by employing a high-power laser and a pressurized gas cell to increase the molecular number density N/V. As long as the pressure is not significantly greater than atmospheric pressure, the gas behaves according to the ideal gas law and number density is proportional to pressure. However, with increasing pressure, complications emerge. An extensive study has been conducted by Petrov & Matrosov on the pressure dependence of Raman signals both theoretically and experimentally comparing N_2, O_2 and CO_2 [55]. The study identified three main correction factors which account for a nonlinear dependence of the gas number density with pressure. First, non-ideal gas behavior results in a compressibility factor that is highly dependent on the type of gas. Second, the increased density leads to modified dielectric properties and thus field intensity. Third, the index of refraction being slightly pressure dependent modifies the numerical aperture of the Raman collection optics [55,56]. The net result of these three factors is that for some gases, for example for carbon dioxide, deviations from linear behavior of order of 20% can be observed when the pressure is raised to around 50 atmospheres [55].

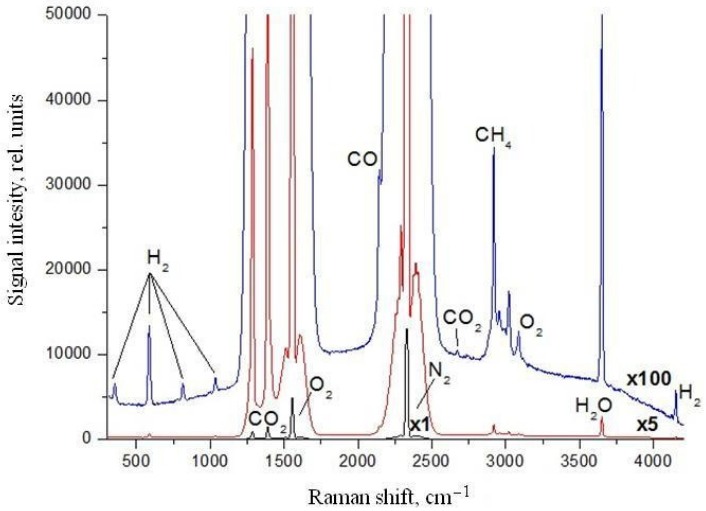

Figure 1: SRS spectrum of the exhaled breath of a smoking person under high pressure of 40 bar . The red and blue curves are scaled by 5 and 100 times respectively with respect to the black curve. Reprinted with permission from Ref. [57]. Copyright 2015 SPIE.

With the understanding that the SRS relationship between number density and pressure can be linearized by appropriate calibration data, Petrov *et al.* have constructed a SRS analyzer operating

under extreme pressurization of near 40 bar. As the pump source, the Raman analyzer employed a diode-pumped solid-state laser emitting 1 W of power at a wavelength of 532 nm. The spectral detection apparatus incorporated a cooled array detector. A measurement with this analyzer that is relevant to breath analysis is shown in Fig. 1. Displayed is the SRS spectrum of breath exhaled by a smoker, revealing clearly signatures of hydrogen, carbon monoxide, and methane well in excess of those in ambient atmospheric air. The limit of detection of the apparatus was estimated at 1 ppm for methane via the band at 2917 cm^{-1}. While increasing gas pressure further to, e.g., 100 bar is in principle possible, other constraints need to be considered. In particular, spectral broadening and spectral shifts would largely negate the advantages of higher number density [55]. However, with advances in laser technology it appears likely that high power lasers with sufficient spectral purity will be available in a more compact form factor than they are today. For instance, the laser power could be increased to at least 10 W compared to 1 W used in the analyzer used for measuring the spectra in Fig. 1.

3.2 Effective interaction length

The effective interaction length, l_{eff}, in Eq. (1) is another critical feature in determining the rate of Raman scattering and thus the limit of detection achievable. When pump laser light is focused in free space, the focal properties are set by intrinsic gaussian beam properties. For a given lens and input beam diameter, the focus cross sectional diameter is inversely proportional to the light's divergence angle, i.e., focusing tighter also reduces the depth of focus proportionately. Waveguiding is a means to circumvent this divergence. It has been accomplished with metal-coated capillary (MCC) tubes whose inside is reflectively coated, as well as with hollow-core photonic crystal fibers (HC-PCFs). The waveguides are filled with a gas sample, and Raman scattered light, generated along the entire length, is collected at one or both ends.

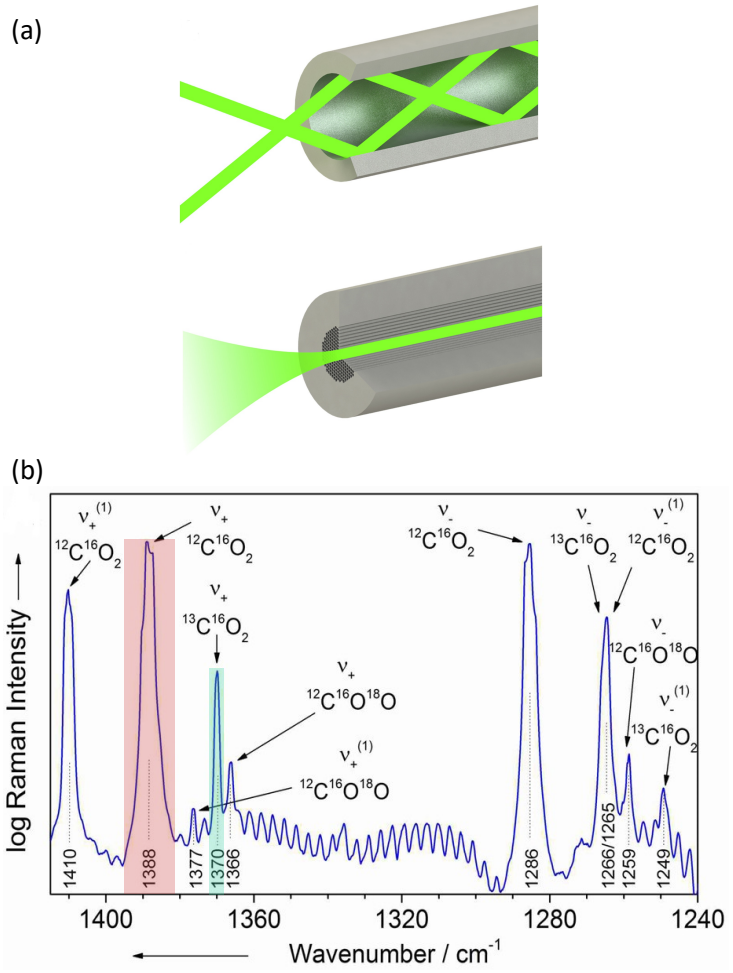

Figure 2: (a) Guided light in MMCs (top) and HC-PCFs (bottom). Reprinted with permission from Ref. [60]. Copyright 2017 Elsevier. (b) High-resolution FERS spectrum of pure CO_2 revealing the presence of natural isotopologues. The colored areas denote the $^{13}CO_2$ (light green) and $^{12}CO_2$ (light brown) isotopologue signatures employed in the determination of χ_{13_C} and χ_{12_C}, respectively, needed for the UBT. Reprinted with permission from Ref. [61]. Copyright 2014 American Chemical Society.

In MCC waveguides, as depicted in Fig. 2(a), light propagation occurs multimodally along the length of the capillary. Typical MCC diameters range from a few hundred micrometers to 1 millimeter, a relatively large size which only moderately impedes sample gas diffusion and thus sample loading time. Capillaries offer an inexpensive and simple solution which has demonstrated for example the measurement of CO_2 peak at 1390 cm^{-1}, achieving a LOD of 143 ppm, utilizing a capillary tube with a 0.8 mm cap, and employing a laser power of 1.5 W at 532 nm. The main drawback of MCCs is high optical losses, limiting the available numerical aperture and the waveguide length to about 65 cm [58].

HC-PCFs offer an alternative with significantly lower losses. HC-PCFs rely on periodic silica/air Bragg structures that propagating light waves encounter in the radial direction. For a range of wavelengths, typically of 50-100 nm, a photonic bandgap results, forbidding light propagation into a certain solid angle. Standard HC-PCFs are commercially available for a range of operating wavelengths. Core mode field diameters can be below 10 micrometers and operation can be almost single mode [Fig. 2(a)].

Optimal fiber lengths are around 50-100 cm as a result of a compromise in losses at the pump wavelength and the Stokes wavelength. In a typical implementation of fiber-enhanced Raman scattering (FERS), pump laser light is focused into one end of a HC-PCF while a pressurized sample gas is flowed through the fiber. Raman scattered light is collected in the same path as the pump, separated by a dichroic filter, and analyzer by a grating spectrometer.

FERS has evolved into an effective analytical tool with an inherent simplicity and robustness, to, e.g., vibrations and other external disturbances [59, 60]. Only a minute amount of sample volume on the nanoliter scale is needed, and rapid real-time trace analysis is possible. In a premixed sample, multigas quantification was demonstrated at levels of 9 ppm, 8 ppm, 4 ppm, 19 ppm, and 0.2 ppm for N_2, O_2, CO_2, N_2O, and CH_4, respectively [61]. In another milestone for FERS, Hanf *et al.* have examined the spectral signatures of naturally abundant carbon dioxide isotopologues [Fig. 2(b)]. These include in particular $^{13}CO_2$ that is detected as part of the UBT in exhaled air. Although it remains to be demonstrated that FERS has the capability to quantify the ratio of the two peaks, indicated in Fig. 2(b), with the needed accuracy, implementation of the UBT with FERS seems likely possible with existing capabilities.

However, considerable practical challenges remain for FERS when it comes to trace detection below the ppm range. Besides the relatively long sample loading times associated with the small core diameters of HC-PCFs, a major obstacle is the generation of background light in the silica cladding, though spatial filtering with a pinhole can alleviate this issue [60–62].

A promising recent development involves the utilization of hollow-core anti-resonant fibers (HC-ARFs). Wang *et al.* have presented a study on FERS based on HC-ARFs which offer a larger core diameter and thus fractionally less modal overlap with the silica cladding [63]. With a 0.27 m long fiber, the detection of hydrogen gas was studied, achieving a limit of detection of 5.4 ppm within an accumulation time of 200 s, demonstrating that HC-ARFs are effective for trace gas detection [63].

3.3 Circulating laser power

Cavity-enhanced Raman scattering (CERS) encompasses an array of techniques designed to augment the interaction between laser light and a gas sample by means of optical cavities. Such approaches typically involve macroscopic optical resonators, microcavities, or multipass cavities [64].

An optical cavity provides recirculation of light such that the flux of photons greatly exceeds that of the freely propagating input light. For example, in a basic two-mirror lossless Fabry-Perot cavity with mirrors of reflectivity R, a circulating power of $P_{circ} = P_{in}/(1 - R)$ results for an input power P_{in}. Given that reflectivities R >99.99% are routinely achievable with modern dielectric coatings, it is possible to generate enhancements of three orders of magnitude or more. Salter *et al.* have realized such enhancement for the purpose of SRS sensing H_2 at a concentration of 460 ppm, generating 10 watts of circulating power using only milliwatts of input power [65]. The cost for this enhancement

is the requirement of a strict resonance condition between the input laser and the optical resonator. In practice, this places considerable constraints on the laser source and mechanical stability of the resonator. In order to couple efficiently to a resonant cavity, a single-spatial-mode laser with a spectral linewidth $\Delta\nu_{laser}$ not exceeding the cavity spectral linewidth $\Delta\nu_{cavity}$ must be maintained frequency-locked with the cavity. Complex stabilization loops such as the Pound-Drever-Hall method are usually employed to provide adequate electro-mechanical or electro-optical feedback. In recent work, Yang *et al.* have implemented such a scheme with a 0.72m-long high-finesse cavity, realizing around 1kW of circulating power with an input power of 240 mW [66]. Highlights from their work, which employs $R = 99.996\%$ reflective mirrors, are reproduced in Fig. 3. A major achievement is the detection of ambient hydrogen at 550 ppb [Fig. 3(b)]. Although this required an exposure time of 40 mins, the detection limit is sufficiently low to implement the HBT for breath analysis. With a cavity linewidth of around 2 kHz, the cavity length needed to be stable at the picometer scale during the feedback timescale, which involved tuning the laser frequency [Fig. 3(a)] [66]. The laser frequency itself required extreme spectral stability at the kHz scale.

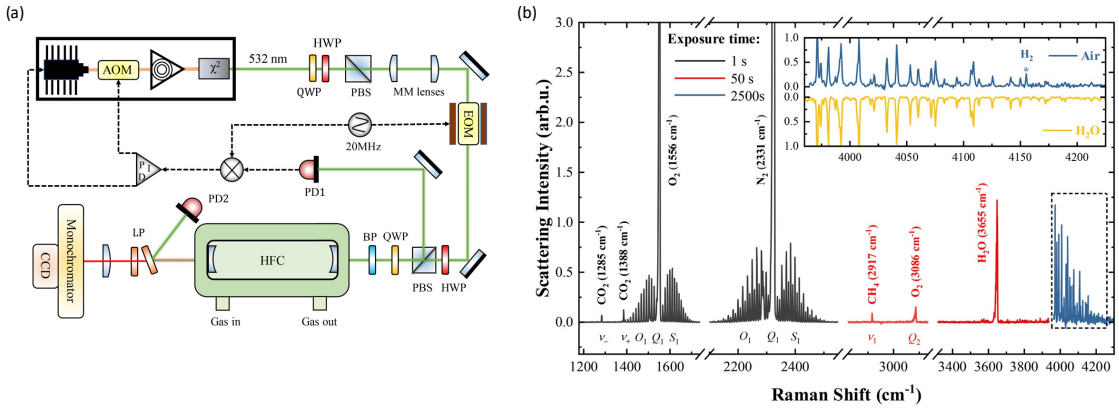

Figure 3: (a) Schematic diagram of CERS with a 0.72m-long high-finesse cavity. Electro-optic modulation and polarization optics provide an error signal with which a feedback loop maintains the laser frequency equal to the cavity resonance frequency. (b) SRS spectrum of ambient air in 1 s (black), 50 s (red) and 2500 s (dark blue) long exposures. The inset reveals a detectable spectral signature of H_2 at 4155 cm^{-1} (550 ppb) within secondary H_2O lines. Reprinted with permission from Ref. [66]. Copyright 2023 American Chemical Society.

Fabry-Perot *micro*-cavities, with mirror separations as little as a micrometer, can provide the additional benefit of Purcell spontaneous emission enhancement [53], with more mechanical robustness than a macroscopic cavity, less stringent requirements on the laser source, and only minute sampling needs that can be easily delivered under considerable pressurization [67]. The Purcell effect, which originates in the modification of vacuum field density of states by the cavity confinement, increases the rate and the fraction of Raman scattered light that can be collected for analysis. However, it comes at the expense of a double laser/cavity resonance, at the pump *and* Stokes frequencies.

An approach with less overhead and less stringent laser requirements is based on *non-resonant* multipass cavities (Fig. 4) [64]. A multipass cavity enables the realization of an increased photon flux

at one or more foci, but in an incoherent manner. Since no constructive interference is involved, as in the Fabry-Perot cavity, the laser source does not need to be spatially single-mode, nor does it need to be of any particular spectral purity.

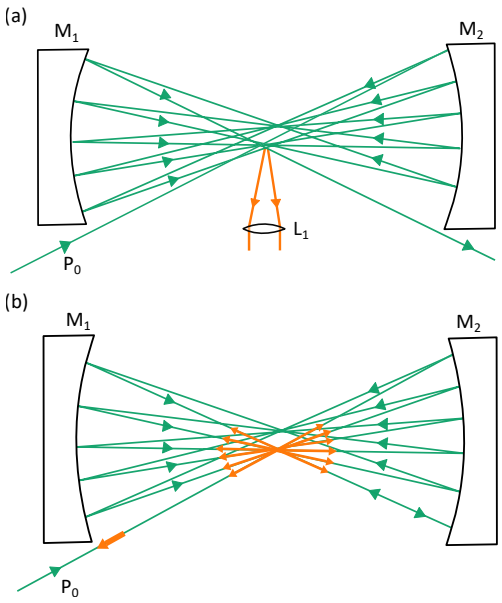

Figure 4: (a) Near-concentric multi-pass cavity built with concave dielectric mirrors M_1 and M_2, with sideways Raman collection. The number of reflections is limited by the ratio of the solid angle of the cavity to that of the focused incoming beam. (b) Near-concentric multipass cavity adjusted to retro-reflect pump light and collect Raman scattered light (orange arrows) co-linearly.

The near-concentric multipass cavity based on two curved mirrors depicted in Fig. 4 is probably the simplest, most studied, and most economical arrangement, although in general a wide variety of configurations are possible, including propagation over unfolded optical paths using combinations of mirrors and lenses [68, 69]. Multipass cavities have been studied extensively in optical absorption cells, for which maximizing path length is the sole goal. In the context of Raman scattering enhancement, creating a long propagation path for the pump beam is not sufficient. Rather, what is most beneficial is for pump beam passes to overlap and refocus in a small volume from which Raman scattered light can be collected.

The traditional method of operating a near-concentric multipass cavity is illustrated in Fig. 4(a). The pump is introduced grazing by—or entering through a hole in—one of the mirrors. A number of reflections occur, whose number is limited by the ratio of the solid angle subtended by the cavity to that subtended by the focused incoming pump beam [70]. The residual pump beam is eventually dumped and Raman scattered light is collected from one of the two foci in a sideways direction. This configuration minimizes background light contributions and avoids pump light returning to the source, which could interfere with its operation.

However, a detection path co-linear with the pump beam offers advantages, as depicted in Fig. 4(b). Instead of collecting sideways, Raman scattered photons are collected along the pump direction using a

dichroic mirror [54]. It is possible to finely adjust the mirror positions and angles such that, upon the last reflection, the beam returns almost exactly the way it entered. This has the consequence that the pump photon flux is doubled, but also that the Raman scattered light is collected in an enlarged solid angle compared to that of the input beam. This effect is indicated in Fig. 4(b) by arrows originating from the foci which represent Raman emission into all pump directions. The net result is a superlinear scaling of the total collected Raman power as a function of the number of reflections [71]. With ultralow-loss mirrors this superlinear growth can be realized to extend the SRS limit of detection well into the ppb range [71].

Nonetheless, the co-linear retro-reflective use of a multipass cavity implies nearly direct return of the pump beam to the laser source. An optical isolator could be used to eliminate the back reflection. However, it can also be leveraged for improved laser power utilization. Gomez-Velez *et al.* have implemented a multipass cavity in which the light source is a spectrally broad multimode blue laser diode [72]. By adding a frequency-selective element such as a volume Bragg grating into the pump beam path, the returning pump beam from the multipass cavity provides spectrally narrowed feedback to the laser diode. It effectively functions as an external cavity diode laser forcing the laser to operate with a linewidth of a few cm^{-1}, with the external cavity length being several meters [73]. High portability is afforded by the simple low cost laser diode, which provides several watts of optical power while only consuming $\sim$10 watts of electrical power [74].

Highlights of feedback-assisted multipass SRS are shown in Fig. 5. Detection of hydrogen in ambient air (550 ppb concentration) is achieved with high signal-to-noise ratio in exposure times of minutes [Fig. 5(a)]. Methane is detectable well into the tens of ppb range [Fig. 5(b)]. Moreover, acetone is detectable in a breath sample [Fig. 5(c)].

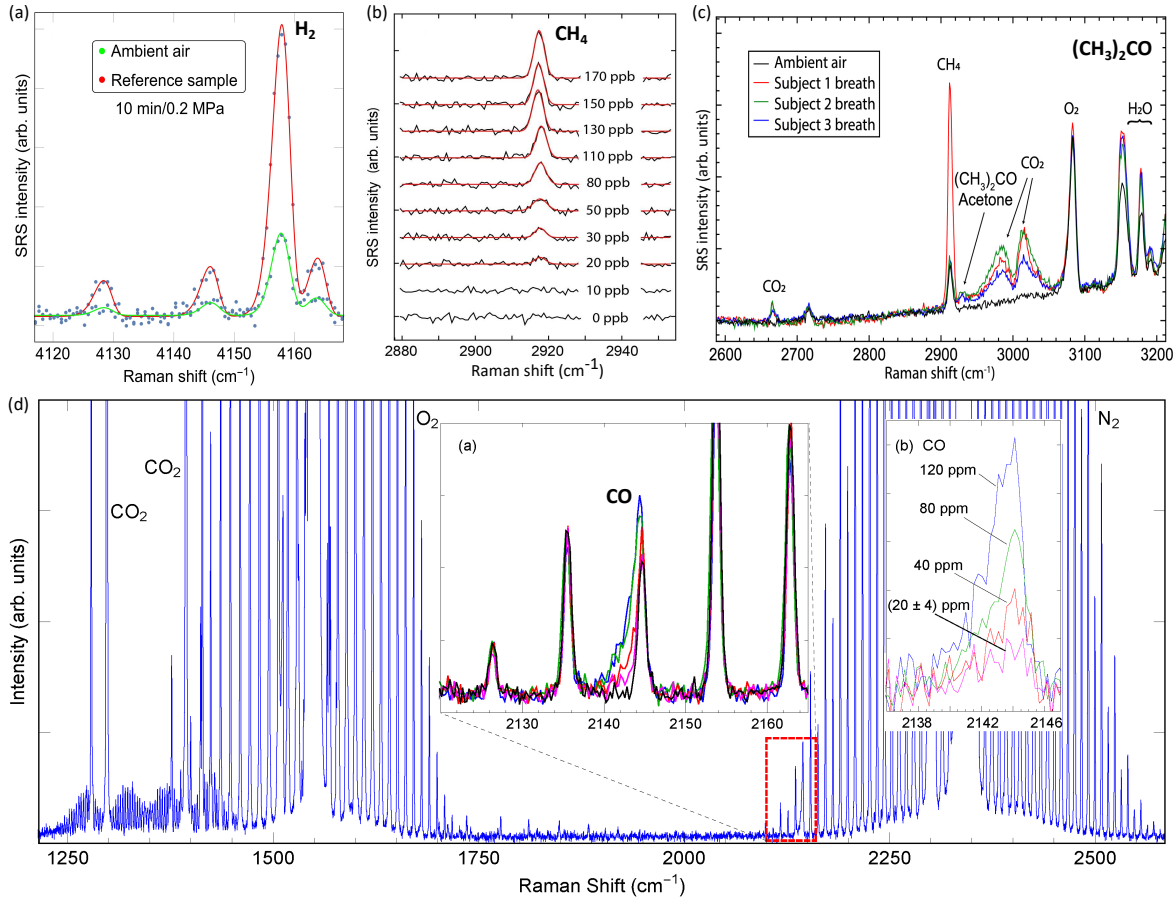

Figure 5: (a) SRS spectrum of ambient air (green) and of a reference sample (red) containing 1.961 ppm of H_2 (10 min integration time and 0.2 MPa of pressure) [75]. (b) SRS spectra of methane of decreasing concentration until noise dominated. Reprinted with permission from Ref. [71]. Copyright 2023 American Chemical Society. (c) Raman spectrum of ambient air and breath samples from three subjects (100 s integration time) [72]. (d) High-resolution SRS spectra of diluted car exhaust gas obtained with Pr:YLF pump laser. Insets show how the CO band, nearly overlapping with the N_2 spectrum, can be extracted down to a concentration of order 10 ppm [76].

Numerous advancements are being explored to make multipass SRS ever more applicable to tasks such as breath analysis. For instance, improving spectral resolution can be decisive for identifying trace species which have vibrational spectral signatures nearly overlapping with those of the predominant species in the gas sample. In Fig. 5(d), multipass SRS data is shown which employed a newly developed Pr:YLF laser producing light directly in the green instead of conventional high power green light sources which do so by way of second-harmonic generation from infrared light. The spectra of Fig. 5(d) show how, with a resolution below 1 cm^{-1}, carbon monoxide signatures can be identified in air down to concentrations as low as 20 ppm. The multipass cavity created an effective circulating power of 16 W, with less than 10 W of electrical input power, implying a high potential for portability.

4 Conclusions and outlook

The rapid progress in SRS enhancement in recent years makes it possible to implement established breath tests such as the UBT and HBT. In addition, primary trace breath analytes such as acetone, ammonia, carbon monoxide and methane, listed in Table 1, are readily quantifiable. While other analytical methods are able to achieve this functionality, the unique strength of SRS is that analytes can be co-detected using the same pump laser and spectrometer. In fact, given achieved limits of detection of order 10 ppb [Fig. 4(b)], it is likely that other hydrocarbons such as isoprene, acetonitrile, etc., will be measurable at the levels needed for diagnostics of, e.g., lung cancer and diabetes [5]. Considerable efforts will still be needed to demonstrate the resilience and durability required of a deployed medical device. Nevertheless, further improvements of SRS for gas detection seem all but certain because of the linear relationship between the SRS rate and laser input power [Eq. (1)], and because depletion of the pump power by the Raman emission is insignificant. Thus, unlocking the full potential of Raman scattering for gas analysis in general—and for breath analysis specifically—boils down to optimal engineering of pump power utilization. Combined with the availability of modern CMOS detectors which do not require cooling, and high efficiency high power laser diodes, SRS is poised to develop into a compact portable tool which can be massively deployed.

Declaration of competing interest

The authors declare that they have no known competing financial interests or personal relationships that could have appeared to influence the work reported in this paper.

Acknowledgements The authors acknowledge financial support from the National Science Foundation (NSF grant No. 2116275).

References

[1] K. Chow, M. Short, H. Zeng, A comparison of spectroscopic techniques for human breath analysis. *Biomed. Spectrosc. and Imag.* **1** (2012) 339-353. https://doi.org/10.3233/BSI-120029.

[2] T. Ligor, J. Szeliga, M. Jackowski, B. Buszewski, Preliminary study of volatile organic compounds from breath and stomach tissue by means of solid phase microextraction and gas chromatography–mass spectrometry. *Journal of Breath Research* **1** (2007) 016001. https://doi.org/10.1088/1752-7155/1/1/016001.

[3] W. Miekisch, J. Schubert, G. Noeldge-Schomburg, Diagnostic potential of breath analysis—focus on volatile organic compounds. *Clinica Chimica Acta.* **347** (2004) 25-39. https://doi.org/10.1016/j.cccn.2004.04.023.

[4] T. Issitt, L Wiggins, M. Veysey, S. Sweeney, W. Brackenbury, K. Redeker, Volatile compounds in human breath: critical review and meta-analysis. *Journal of Breath Research*. **16** (2022) 024001. https://doi.org/10.1088/1752-7163/ac5230.

[5] S. Das, S. Pal, M. Mitra, Significance of Exhaled Breath Test in Clinical Diagnosis: A Special Focus on the Detection of Diabetes Mellitus. *Journal of Medical and Biological Engineering*. **36** (2016) 605-624. https://doi.org/10.1007/s40846-016-0164-6.

[6] X. Zhang, P. Wargocki, Z. Lian, C. Thyregod, Effects of exposure to carbon dioxide and bioeffluents on perceived air quality, self-assessed acute health symptoms, and cognitive performance. *Indoor Air*. **27** (2017) 47-64. https://doi.org/10.1111/ina.12284.

[7] A. Hartmann, R. Strzoda, R. Schrobenhauser, R. Weigel, CO2 sensor for mainstream capnography based on TDLAS. *Applied Physics B*. **116** (2014) 1023-1026.

[8] B. Walsh, D. Crotwell, R. Restrepo, Capnography/Capnometry During Mechanical Ventilation: 2011. *Respiratory Care*. **56** (2011) 503-509. https://doi.org/10.4187/respcare.01175.

[9] S. Deveci, F. Deveci, Y. Açik, A. Ozan, The measurement of exhaled carbon monoxide in healthy smokers and non-smokers. *Respiratory Medicine*. **98** (2004) 551-556. https://doi.org/10.1016/j.rmed.2003.11.018.

[10] R. Zegdi, D. Perrin, M. Burdin, R. Boiteau, A. Tenaillon, Increased endogenous carbon monoxide production in severe sepsis. *Intensive Care Medicine*. **28** (2002) 793-796. https://doi.org/10.1007/s00134-002-1269-7.

[11] A. Lal, L. Patterson, A. Goldrich, A. Marsh, Point-of-care end-tidal carbon monoxide reflects severity of hemolysis in sickle cell anemia. *Pediatric Blood & Cancer*. **62** (2015) 912-914. https://doi.org/10.1002/pbc.25447.

[12] A. Eisenmann, A. Amann, M. Said, B. Datta, M. Ledochowski, Implementation and interpretation of hydrogen breath tests. *Journal Of Breath Research*. **2** (2008) 046002. https://doi.org/10.1088/1752-7155/2/4/046002.

[13] M. Levitt, J. Furne, M. Kuskowski, J. Ruddy, Stability of Human Methanogenic Flora Over 35 Years and a Review of Insights Obtained From Breath Methane Measurements. *Clinical Gastroenterology And Hepatology*. **4** (2006) 123-129. https://doi.org/10.1016/j.cgh.2005.11.006.

[14] V. Ruzsányi, M. Kalapos, Breath acetone as a potential marker in clinical practice*. *Journal Of Breath Research*. **11** (2017) 024002. https://doi.org/10.1088/1752-7163/aa66d3.

[15] G. Hancock, S. Sharma, M. Galpin, D. Lunn, C. Megson, R. Peverall, G. Richmond, G. Ritchie, K. Owen, The correlation between breath acetone and blood betahydroxybutyrate in individuals

with type 1 diabetes. *Journal Of Breath Research*. **15** (2020) 017101. https://doi.org/10.1088/1752-7163/abbf37.

[16] C. Turner, P. Španěl, D. Smith, A longitudinal study of ammonia, acetone and propanol in the exhaled breath of 30 subjects using selected ion flow tube mass spectrometry, SIFT-MS. *Physiological Measurement*. **27** (2006) 321. https://doi.org/10.1088/0967-3334/27/4/001.

[17] A. Aguilar, E. Forzani, N. Tao, L. Nagahara, I. Amlani, R. Tsui, A Breath Ammonia Sensor Based on Conducting Polymer Nanojunctions. *IEEE Sensors Journal*. **8** (2008) 269-273. http://dx.doi.org/10.1109/JSEN.2007.913137.

[18] S. Davies, P. Spanel, D. Smith, Quantitative analysis of ammonia on the breath of patients in end-stage renal failure. *Kidney International*. **52** (1997) 223-228. https://doi.org/10.1038/ki.1997.324.

[19] Z. Endre, J. Pickering, M. Storer, W. Hu, K. Moorhead, R. Allardyce, D. McGregor, J. Scotter, Breath ammonia and trimethylamine allow real-time monitoring of haemodialysis efficacy. *Physiological Measurement*. **32** (2010) 115. https://doi.org/10.1088/0967-3334/32/1/008.

[20] P. Mazzone, Analysis of Volatile Organic Compounds in the Exhaled Breath for the Diagnosis of Lung Cancer. *Journal Of Thoracic Oncology*. **3** (2008) 774-780. https://doi.org/10.1097/jto.0b013e31817c7439.

[21] E. Popov, A. Polishchuk, A. Kovalev, V. Vitkin, Raman Spectroscopy for Urea Breath Test. *Biosensors*. **13** (2023). https://doi.org/10.3390/bios13060609.

[22] A. Berger, Helicobacter pylori breath tests. *BMJ : British Medical Journal*. **324** (2002) 1263. https://doi.org/10.1136/bmj.324.7348.1263.

[23] S. Rana, A. Malik, Hydrogen Breath Tests in Gastrointestinal Diseases. *Indian Journal Of Clinical Biochemistry*. **29** (2014) 398-405. https://doi.org/10.1007/s12291-014-0426-4.

[24] Uday C Ghoshal, How to Interpret Hydrogen Breath Tests. *Journal Of Neurogastroenterology And Motility*. **17** (2011) 312-317. https://doi.org/10.5056/jnm.2011.17.3.312.

[25] M. Olshina, M. Sharon, Mass spectrometry: a technique of many faces. *Quarterly Reviews Of Biophysics*. **49** (2016) e18. https://doi.org/10.1017%2FS0033583516000160.

[26] G. Glish, R. Vachet, The basics of mass spectrometry in the twenty-first century. *Nature Reviews Drug Discovery*. **2** (2003,2) 140-150. https://doi.org/10.1038/nrd1011.

[27] G. Guiochon, C. Guillemin, Gas chromatography. *Review Of Scientific Instruments*. **61** (1990) 3317-3339. https://doi.org/10.1063/1.1141631.

[28] G. Eiceman, J. Gardea-Torresdey, E. Overton, K. Carney, F. Dorman, Gas Chromatography. *Analytical Chemistry*. **74** (2002) 2771-2780. https://doi.org/10.1021/ac0400663.

[29] R. Blake, P. Monks, A. Ellis, Proton-Transfer Reaction Mass Spectrometry. *Chemical Reviews.* **109** (2009) 861-896. https://doi.org/10.1021/cr800364q.

[30] B.Yuan, A. Koss, C. Warneke, M. Coggon, K. Sekimoto, J. Gouw, Proton-Transfer-Reaction Mass Spectrometry: Applications in Atmospheric Sciences. *Chemical Reviews.* **117** (2017) 13187-13229. https://doi.org/10.1021/acs.chemrev.7b00325.

[31] C. Hastie, A. Thompson, M. Perkins, V. Langford, M. Eddleston, N. Homer, Selected Ion Flow Tube-Mass Spectrometry (SIFT-MS) as an Alternative to Gas Chromatography/Mass Spectrometry (GC/MS) for the Analysis of Cyclohexanone and Cyclohexanol in Plasma. *ACS Omega.* **6** (2021) 32818-32822. https://doi.org/10.1021/acsomega.1c03827.

[32] M. Mäkinen, O. Anttalainen, M. Sillanpää, Ion Mobility Spectrometry and Its Applications in Detection of Chemical Warfare Agents. *Analytical Chemistry.* **82** (2010) 9594-9600. https://doi.org/10.1021/ac100931n.

[33] J. Dodds, E. Baker, Ion Mobility Spectrometry: Fundamental Concepts, Instrumentation, Applications, and the Road Ahead. *Journal Of The American Society For Mass Spectrometry* **30** (2019) 2185-2195. https://doi.org/10.1007/s13361-019-02288-2.

[34] P. Wang, W. Chen, F. Wan, J. Wang, J. Hu, Cavity-enhanced Raman spectroscopy with optical feedback frequency-locking for gas sensing. *Opt. Express*, **16** (2019) 30517-30529. https://doi.org/10.1364/oe.27.033312.

[35] F. Aemisegger, P. Sturm, P. Graf, H. Sodemann, S. Pfahl, A. Knohl, H. Wernli, Measuring variations of δ 18 O and δ 2 H in atmospheric water vapour using two commercial laser-based spectrometers: an instrument characterisation study. *Atmos. Meas. Tech.* **5** (2012) 1491-1511. https://doi.org/10.5194/amt-5-1491-2012.

[36] T. Iwata, T. Katagiri, Y. Matsuura, Real-Time Analysis of Isoprene in Breath by Using Ultraviolet-Absorption Spectroscopy with a Hollow Optical Fiber Gas Cell. *Sensors.* **16** (2016). https://doi.org/10.3390/s16122058.

[37] M. Metsälä, Optical techniques for breath analysis: from single to multi-species detection. *Journal Of Breath Research.* **12** (2018) 027104. https://doi.org/10.1088/1752-7163/aa8a31.

[38] J. Kuhn, U. Platt, N. Bobrowski, T. Wagner, Towards imaging of atmospheric trace gases using Fabry–Pérot interferometer correlation spectroscopy in the UV and visible spectral range. *Atmospheric Measurement Techniques.* **12** (2019) 735-747. https://doi.org/10.5194/amt-12-735-2019.

[39] P. Geiko, V. Korolkov, V. Tatur, Development and Implementation of UV Absorption Gas Analysis Techniques for Ecological Monitoring of the Atmosphere. *Atmospheric And Oceanic Optics.* **35** (2022) 443-449. https://doi.org/10.15372/AOO20220201.

[40] J. Galewsky, H.C. Steen-Larsen, R.D. Field, J. Worden, C. Risi, C., M. Schneider, Stable isotopes in atmospheric water vapor and applications to the hydrologic cycle. *Rev. Geophys.* **54** (2016) 809-865. https://doi.org/10.1002/2015RG000512.

[41] Ciaffoni, L., Hancock, G., Harrison, J. J., van Helden, J-P. H., Langley, C. E., Peverall, R., Ritchie, G. A. D. & Wood, S., Demonstration of a mid-infrared cavity enhanced absorption spectrometer for breath acetone detection. *Anal. Chem.* **85** (2013) 846-850. https://doi.org/10.1021/ac3031465.

[42] Wang, J., Tian, X., Dong, Y., Zhu, G., Chen, J., Tan, T., Liu, K., Chen, W. & Gao, X., Enhancing off-axis integrated cavity output spectroscopy (OA-ICOS) with radio frequency white noise for gas sensing. *Opt. Express* **27** (2019) 30517-30529. https://doi.org/10.1364/oe.27.030517.

[43] Van Helden, J. H., Lang, N, Macherius, U., Zimmermann, H. & Röpcke, J., Sensitive trace gas detection with cavity enhanced absorption spectroscopy using a continuous wave external-cavity quantum cascade laser. *Appl. Phys. Lett.* **13** (2013) 131114. https://doi.org/10.1063/1.4823545.

[44] Tans, P. P., Crotwell, A. M. & Thoning, K. W., Abundances of isotopologues and calibration of CO2 greenhouse gas measurements. *Atmos. Meas. Tech.* **10** (2017) 2669-2685. https://doi.org/10.5194/amt-10-2669-2017.

[45] Sonnenschein, V., Terabayashi, R., Tomita, H., Kato, S., Hayashi, N., Takeda, S., Jin, L., Yamanaka, M., Nishizawa, N., Sato, A., Yoshida, K. & Iguchi, T., A cavity ring-down spectrometer for study of biomedical radiocarbon-labeled samples, *J. Appl. Phys.* **124** (2018) 033101. https://doi.org/10.1063/1.5041015.

[46] Brenna, J. T., Corso, T. N., Tobias, H. J. & Caimi, R. J., High-precision continuous-flow isotope ratio mass spectrometry. *Mass Spectrom. Rev.* **16** (1997) 227-258. https://doi.org/10.1002/(sici)1098-2787(1997)16:5%3C227::aid-mas1%3E3.0.co;2-j.

[47] Modak, A. Stable isotope breath tests in clinical medicine: a review. *Journal Of Breath Research.* **1**(2007) 014003. https://doi.org/10.1088/1752-7155/1/1/014003.

[48] Lee, J., Kim, M., Soltis, I., Lee, S. & Yeo, W. Advances in Electrochemical Sensors for Detecting Analytes in Biofluids. *Advanced Sensor Research.* **2** (2023) 2200088. https://doi.org/10.1002/adsr.202200088.

[49] Baranwal, J., Barse, B., Gatto, G., Broncova, G. & Kumar, A. Electrochemical Sensors and Their Applications: A Review. *Chemosensors.* **10** (2022). https://doi.org/10.3390/chemosensors10090363.

[50] Gaffney, E., Lim, K. & Minteer, S. Breath biosensing: using electrochemical enzymatic sensors for detection of biomarkers in human breath. *Current Opinion In Electrochemistry.* **23** (2020) 26-30. https://doi.org/10.1016/j.coelec.2020.02.014.

[51] Niklas, C., Wackerbarth, H. & Ctistis, G. A Short Review of Cavity-Enhanced Raman Spectroscopy for Gas Analysis. *Sensors*. **21** (2021). https://doi.org/10.3390/s21051698.

[52] Orlando, A., Franceschini, F., Muscas, C., Pidkova, S., Bartoli, M., Rovere, M. & Tagliaferro, A. A Comprehensive Review on Raman Spectroscopy Applications. *Chemosensors*. **9** (2021). https://doi.org/10.3390/chemosensors9090262.

[53] Petrak, B., Djeu, N. & Muller, A. Purcell-enhanced Raman scattering from atmospheric gases in a high-finesse microcavity. *Phys. Rev. A*. **89**, 023811 (2014). https://doi.org/10.1103/PhysRevA.89.023811.

[54] Chibirev, I., Mazzoleni, C., Van der Voort, D., Borysow, J. & Fink, M. Raman spectrometer for field determination of H2O in natural gas pipelines. *Journal Of Natural Gas Science And Engineering*. **55** (2018) pp. 426-430. https://doi.org/10.1016/j.jngse.2018.05.015.

[55] Petrov, D. & Matrosov, I. Pressure dependence of the Raman signal intensity in high-pressure gases. *Journal Of Raman Spectroscopy*. **48** (2017) 474-478. https://doi.org/10.1002/jrs.5062.

[56] Tanichev, A. & Petrov, D. Pressure broadening in Raman spectra of CH4–N2, CH4–CO2, and CH4–C2H6 gas mixtures. *Spectrochimica Acta Part A: Molecular And Biomolecular Spectroscopy*. **291** (2023) 122396. https://doi.org/10.1016/j.saa.2023.122396.

[57] Petrov, D., Matrosov, I. & Tikhomirov, A. Raman gas analyzer applicability to monitoring of gaseous air pollution. *21st International Symposium Atmospheric And Ocean Optics: Atmospheric Physics*. **9680** (2015) 700-704. https://doi.org/10.1117/12.2205330.

[58] James, T., Rupp, S. & Telle, H. Trace gas and dynamic process monitoring by Raman spectroscopy in metal-coated hollow glass fibres. *Anal. Methods*. **7**, (2015) 2568-2576. http://doi.org/10.1039/C4AY02597K.

[59] Knebl, A., Domes, R., Yan, D., Popp, J., Trumbore, S. & Frosch, T. Fiber-Enhanced Raman Gas Spectroscopy for 18O–13C-Labeling Experiments. *Analytical Chemistry*. **91** (2019) 7562-7569. https://doi.org/10.1021/acs.analchem.8b05684.

[60] Knebl, A., Yan, D., Popp, J. & Frosch, T. Fiber enhanced Raman gas spectroscopy. *TrAC Trends In Analytical Chemistry*. **103** (2018) 230-238. https://doi.org/10.1021/acs.analchem.7b03209.

[61] Hanf, S., Keiner, R., Yan, D., Popp, J. & Frosch, T. Fiber-Enhanced Raman Multigas Spectroscopy: A Versatile Tool for Environmental Gas Sensing and Breath Analysis. *Analytical Chemistry*. **86** (2014) 5278-5285. https://doi.org/10.1021/ac404162w.

[62] Sieburg, A., Knebl, A., Jacob, J. & Frosch, T. Characterization of fuel gases with fiber-enhanced Raman spectroscopy. *Analytical And Bioanalytical Chemistry*. **411** (2019) 7399 - 7408. https://doi.org/10.1007/s00216-019-02145-x.

[63] Wang, J., Chen, W., Wang, P., Zhang, Z., Wan, F., Zhou, F., Song, R., Wang, Y. & Gao, S. Fiber-enhanced Raman spectroscopy for highly sensitive H2 and SO2 sensing with a hollow-core anti-resonant fiber. *Opt. Express.* **29** (2021) 32296-32311. https://doi.org/10.1364/OE.437693.

[64] Pinyi Wang & Hu, J. A review of cavity-enhanced Raman spectroscopy as a gas sensing method. *Applied Spectroscopy Reviews.* **55** (2020) 393-417. https://doi.org/10.1080/05704928.2019.1661850.

[65] Salter, R., Chu, J. & Hippler, M. Cavity-enhanced Raman spectroscopy with optical feedback cw diode lasers for gas phase analysis and spectroscopy. *Analyst.* **137**, (2012) 4669-4676. https://doi.org/10.1039/C2AN35722D.

[66] Yang, Q., Tan, Y., Qu, Z., Sun, Y., Liu, A. & Hu, S. Multiple Gas Detection by Cavity-Enhanced Raman Spectroscopy with Sub-ppm Sensitivity. *Analytical Chemistry.* **95** (2023) 5652-5660. https://doi.org/10.1021/acs.analchem.2c05432.

[67] Gomez Velez, J. & Muller, A. Purcell-enhanced microcavity Raman scattering from pressurized gases. *Applied Physics Letters.* **112**, (2018) 041107. https://doi.org/10.1063/1.5016180.

[68] Shen, C., Wen, C., Huang, X. & Long, X. A Versatile Multiple-Pass Raman System for Industrial Trace Gas Detection. *Sensors.* **21** (2021). https://doi.org/10.3390/s21217173.

[69] Hill, R., Mulac, A. & Hackett, C. Retroreflecting multipass cell for Raman scattering. *Appl. Opt..* **16** (1977) 2004-2006. https://doi.org/10.1364/AO.16.002004.

[70] Petrov, D. Multipass optical system for a Raman gas spectrometer. *Appl. Opt..* **55**,(2016) 9521-9525. https://doi.org/10.1364/AO.55.009521.

[71] Singh, J.; Muller, A. Ambient Hydrocarbon Detection with an Ultra-Low-Loss Cavity Raman Analyzer. *Anal. Chem.* **2023**, *95* 3703–3711. https://doi.org/10.1021/acs.analchem.2c04707.

[72] Velez, J. & Muller, A. Trace gas sensing using diode-pumped collinearly detected spontaneous Raman scattering enhanced by a multipass cell. *Opt. Lett..* **45** (2020) 133-136. https://doi.org/10.1364/OL.45.000133.

[73] Velez, J. & Muller, A. Spontaneous Raman scattering at trace gas concentrations with a pressurized external multipass cavity. *Measurement Science And Technology.* **32**, (2021) 045501. https://doi.org/10.1088/1361-6501/abd11e.

[74] Singh, J. & Muller, A. Isotopic trace analysis of water vapor with multipass cavity Raman scattering. *Analyst.* **146**, (2021) 6482-6489. http://doi.org/10.1039/D1AN01254A.

[75] Singh, J. & Muller, A. High-Precision Trace Hydrogen Sensing by Multipass Raman Scattering. *Sensors.* **23** (2023). https://doi.org/10.3390/s23115171.

[76] Arachchige, C. & Muller, A. Narrow-Linewidth Pr:YLF Laser for High-Resolution Raman Trace Gas Spectroscopy. *Spectroscopy Journal*. **1** (2023) 86-97. https://doi.org/10.3390/spectroscj1020008.